16th Australasian Fluid Mechanics Conference
Crown Plaza, Gold Coast, Australia
2-7 December 2007

Non-linear growth of short-wave instabilities in a Batchelor vortex pair

K. Ryan and G. J. Sheard

Fluids Laboratory for Aeronautical and Industrial Research (FLAIR)
Department of Mechanical Engineering,
Monash University, Australia.

Abstract

Recent investigations have identified a variety of instability modes which may develop to enhance dispersion of co- and counter-rotating vortex pairs. This has application in the aviation industry, where an aircraft's trailing vortices pose a significant hazard for other nearby aircraft. Batchelor vortices adopt the radial velocity field of Lamb – Oseen vortices, but with an axial velocity component through the core of the vortex, and are often used to represent vortices within an aircraft wake. Recently, the vortex swirl ratio of the Batchelor vortex pair has been identified as a key parameter which may be used to select the mode of instability which develops. Several modes have recently been identified via linear stability analysis.

This study extends these prior investigations by considering the non-linear growth of the three-dimensional instabilities acting to disperse the vortex pair. Here, we validate prior linear instability investigations, and compare and contrast the relative ability of several instability modes to achieve improved vortex dispersion. The study has been conducted using a high-order, three-dimensional spectral element method to solve the time-dependent incompressible Navier – Stokes equations. The study is conducted at a circulation Reynolds number of 2 800.

Introduction

Large commercial aircraft, through the generation of coherent, energetic trailing vortices, can pose a significant risk to other aircraft in their vicinity ([15]) . Downstream of the aircraft, the vortex sheet comprising the wake develops to form a counter-rotating vortex pair, each of which have an additional velocity component in line with the axis of the vortex. This velocity component is generated by the forward motion of the aircraft through the air. The vortices persist well after the initiating aircraft has departed and may alter the flight characteristics of trailing aircraft. The strength and time to dissipation of the trailing vortices are proportional to the weight, size and lift coefficient of the initiating aircraft. The flight space close to airports pose a significant risk due to the density of aviation traffic and the high lift coefficients aircraft employ during takeoff and landing. In order to maintain safety, airports require that a minimum distance be maintained between aircraft utilizing a single runway ([12]). This minimum distance requirement imposes an upper limit to the number of aircraft which may safely use airport facilities over a given period of time ([15]).

The recent introduction of larger commercial aircraft imposes more pressure on the fluid dynamics community to resolve this issue. The past forty years has witnessed considerable research effort to understand the fundamental nature of aircraft wakes with an aim to enhance the dissipation of the strong, coherent vortical structures within them ([15]). To date, little of this research effort has translated into practical devices to alleviate this problem.

Crow [2] identified a large wavelength perturbation mechanism which induced the improved dissipation of the vortex structure in the wake of an aircraft. However, while it was noted that the mechanism induced vortex annihilation 20 times faster than viscous dissipation alone, the large wavelength instability still requires significant time to develop.

More recently, both experimental and numerical investigations have considered the instability mechanisms for counter-rotating vortex pairs for vortices with no axial velocity component ([10, 5]) . For both cases, a short-wave, sinusoidal oscillation was found to grow in each vortex, corresponding to a resonance of the (-1,1) Kelvin mode coupling in each vortex. Le Dizès & Williamson [10] observed an elliptic Kelvin mode superimposed on the large wavelength, Crow instability. They observed that the addition of the short wavelength instability resulted in a 20% increase in the normalized growth rate at a Reynolds number, $Re = 2800$. Where the Reynolds number is defined based on the circulation within each vortex as $Re = \Gamma/\nu$ (Γ is the circulation of an individual vortex and ν is the kinematic viscosity). Le Dizès & Williamson [10] identified secondary vortices which evolved during the non-linear growth period of the (-1,1) Kelvin mode. They found that the secondary vortices promoted mixing between the two vortices which greatly enhanced dissipation of both vortices. Their work was validated by direct numerical simulations conducted by [5]. Meunier & Leweke [11] found a similar result when considering a co-rotating vortex pair. However, no short-wave elliptic instability was observed to develop in the presence of even a small axial velocity component by [10, 5] or [11]; hence these findings were not directly applicable to the aircraft wake problem.

The short-wave instability mode identified by [10] is only one of several Kelvin type instabilities which may propagate within a vortex ([3]). Le Dizès & Laporte [8] investigated the effect of adding an axial velocity component on the form of inviscid normal instability modes (Kelvin modes) which may grow in the presence of the Batchelor vortex pair, where each vortex (expressed in cylindrical coordinates - r, θ, z) is of the form

$$\omega_z = \frac{\Gamma}{\pi a_0^2} e^{r^2/a_0^2}, \tag{1}$$

$$W = \frac{W_0 \Gamma a_0}{2\pi a^2} e^{r^2/a_0^2}. \tag{2}$$

Here ω_z is the axial vorticity component, W is the axial velocity component, a is the characteristic core radius of the vortex (a_0 is the core radius at time $t = 0$) , and W_0 is the axial velocity coefficient, defined as

$$W_0 = \frac{\hat{W}}{\hat{u_\theta}} = \frac{1}{q}, \tag{3}$$

where $\hat{u_\theta}$ is the maximum azimuthal velocity component, $\hat{W}$ is the maximum axial velocity component and q is the swirl number. Such a vortex profile was first derived by [1] as the

asymptotic solution to the linearized Navier-Stokes equation for a trailing line vortex profile far downstream of an aircraft. For the case where $W_0 = 0$, the vortex profile (equation 1) reverts to a Lamb – Oseen type.

Le Dizès & Laporte [8]'s investigation identified several other Kelvin mode pairs (apart from mode [-1,1] identified in earlier studies) which could occur in the presence of an axial velocity. A further investigation by [6] analytically determined the normalized growth rates of the short-wave Kelvin mode pairs as a function of W_0 and the axial wavenumber k. Analytically, this investigation was initially conducted in an inviscid fluid ($Re = \infty$). The effect of a viscous fluid was considered by introducing a damping effect on the growth rates of the instability modes. In particular the Kelvin mode pair (-2,0) was identified to have a high growth rate for a range of axial velocities. It has been suggested that this mode may enhance the dissipation of the vortex pair in the presence of an axial velocity ([6]).

The analytical work of [6] has been validated in two ways. Lacaze et al. [6] validated their findings by solving the linearized Navier Stokes equations for the growth of a random perturbation field which was overlayed on a base flow comprising of a Batchelor vortex pair. The computational findings were found to agree closely with the analytical estimates. More recent investigations by [13] have also identified both Kelvin modes using DNS; their findings agree well with the work of [8] and [6]. However, to date the non-linear growth of mode [-2,0] has not been considered in detail. This is important, as [10] noted that it was the secondary vortices, apparent only during the non-linear growth of mode [-1,1] which was crucial to the enhanced dissipation of the vortex pair. A number of questions naturally arise which this paper aims to address:

- Does mode [-2,0] provide dissipation rates in the non-linear regime comparable to mode [-1,1]?
- Does mode [-2,0] exhibit secondary vortices which may enhance vortex dissipation?
- Is inter-vortical mixing enhanced by the development of mode [-2,0]?

The current work aims to address these questions by comparing the structure of mode [-1,1] to mode [-2,0] through both the linear and non-linear growth regimes. In particular, the dissipation of coherent vortex structures in the wake for each mode will be considered.

Flow Field Description

In this study two counter-rotating Batchelor vortices, each of characteristic radius a, are placed a distance b apart. Each vortex imposes a weak external strain field on the other, ε_0 (for example see [14, 9]). This paper restricts its attention to the study of counter rotating vortices of equal circulation magnitude. In isolation, a Batchelor vortex represents a stationary solution to the Euler equations, and a complete solution to the Navier – Stokes equations. A vortex with a Gaussian profile is a known global attractor of any two-dimensional axisymmetric vortex (see for example [9]). The Gaussian profile has the advantage over other possible profiles, because it is unaffected by viscous diffusion. Viscosity only acts to modify the radius of the vortex, which evolves linearly in time ([9])) and has been shown to evolve as

$$a(t) = \sqrt{a_0^2 + 8\pi t^* b^2 Re} \tag{4}$$

Here a_0 is the initial radius of the vortex, t^* is the normalised time unit defined as

$$t^* = \frac{t}{t_c}, \tag{5}$$

and t_c is the characteristic time for instability growth defined as

$$t_c = \frac{2\pi b^2}{\Gamma}. \tag{6}$$

Assuming a sufficiently large Reynolds number, the vortex core size may be considered constant over time. Throughout this study, the Reynolds number and the normalised vortex separation distance were held constant at $Re = 2800$, and $a/b = 0.25$ respectively, corresponding to the experiments performed by [10], and the simulations conducted by [5].

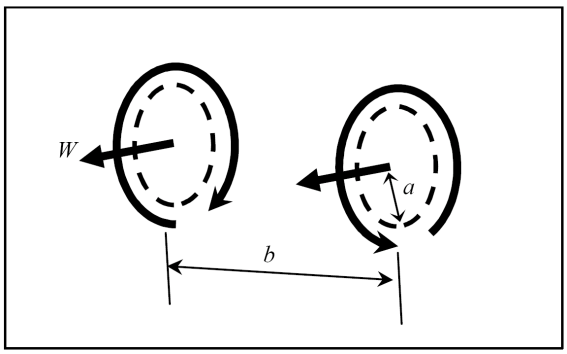

Figure 1: Schematic representation of the flow field under investigation. Here, a is the characteristic core radius, b is the separation distance between the vortex cores and W is the velocity component parrallel to the axial direction.

Numerical Technique

A DNS technique was utilized to investigate both the linear and non-linear growth of the Kelvin modes of interest. A high – order method was used for this purpose, the domain is subdivided in the axial direction into a series of planes. A spectral-element method was used for the spatial discretization within each plane. The method employs high-order tensor-product Lagrangian polynomials as shape functions within each element. A Fourier expansion of the velocity and pressure fields was employed in the axial direction across the planes. The three-dimensional method extends the two dimensional spectral element method by using a global Fourier spectral discretization in the third dimension. This approach has been employed previously for the case of the flow past a circular cylinder by [16], among many others. The global spectral approach has the advantage of spectral convergence, however the boundary conditions in the axial direction are restricted to be periodic.

The spatial discretization consists of 64 equi-spaced planes in the span-wise direction, each consisting of an identical spectral-element mesh. The flow variables are transformed into Fourier space in the span-wise direction for each node on the spectral element mesh using a fast Fourier transform. This decouples the problem into a set of 64 Fourier modes which are then solved independently for the linear operators. The time integration uses a three-step time-splitting method and achieves second-order time accuracy, and is described completely in [4] The spatial accuracy was determined at run time by specifying the order of the tensor-product of interpolating polynomi-

als within each macro-element. In all the simulations quoted herein, 700 macro-elements were employed with 8^{th} order polynomial interpolants. A square domain was employed with a domain length and width of 40 vortex diameters.

If the two vortices are localized and sufficiently far apart, each vortex may be represented as a point vortex. This representation provides the inviscid dynamics of the system and, if the viscous effects are negligible, to leading order may be used to represent a real system. Using this concept, the two-dimensional dynamics of the vortex system is reduced to determining the evolution of two point vortices of circulation Γ_1 and Γ_2, separated by a distance b. For the case of two counter-rotating vortices of equal magnitude (i.e. assuming $\Gamma_1 = -\Gamma_2$ and $|\Gamma_{1,2}| = \Gamma$) the two vortices induce a constant velocity along a straight line, perpendicular to the line connecting them, which is given by the equation:

$$V = \frac{\Gamma}{2\pi b}. \tag{7}$$

In the present simulations, the self-advection speed of the vortex pair is subtracted such that the vortices remain within the computational domain.

Initial Conditions and the Two-Dimensional Relaxation Process

Simulations commence with a pair of identical vortices, each with a profile described by equation 1 and 2. Such a flow field is not a solution to the Navier – Stokes equations, and the vortex pair have to 'relax' to a physical solution. The relaxation process is well documented (for example see [14, 9]) allowing the strain field induced from one vortex to affect the profile of the other until a self-similar solution is converged upon for each vortex. The process is inviscid, and is conducted at a Reynolds number of 20 000 such that the vortex core radii do not increase appreciably during the process. The Reynolds number is then reduced to 2 800 for the three dimensional investigation. The relaxation process was conducted on one plane using a two-dimensional spectral element method. At the conclusion of the relaxation process the plane was then copied across all 64 planes for the three-dimensional simulations. At the end of the process each vortex has an elliptical profile as shown in figure 2.

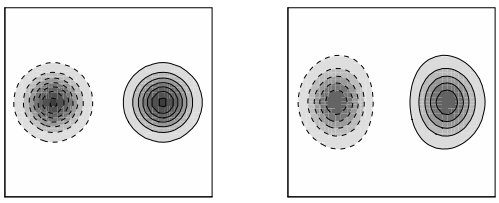

(a) (b)

Figure 2: Vorticity contours, ω_z, showing the evolution of the initial flow field to the final, 'relaxed', elliptical profile of each vortex core used for later three-dimensional simulations. Figure (a) shows the initial field comprising two vortices of Gaussian profile. Figure (b) shows the flow field at the completion of the relaxation process.

Results: Three-Dimensional Simulations

While several values of W_0 were considered for this investigation, the findings for only two of them will be discussed here. These two modes have the highest growth rate, and hence those of most interest. The first simulation reported is the previously studied case of the Batchelor vortex pair in the absence of an axial velocity component (a Lamb – Oseen vortex), the results of which allow comparison of the current numerical technique with several other investigations. The second case is for $W_0 = 0.5$, this allows direct comparison with the findings of Lacaze et al. (2006). In each case the axial wave number was chosen such that the region of maximum growth rate was targeted. Therefore, for the case where $W_0 = 0, k = 2.3$ and for $W_0 = 0.482, k = 1.9$.

Mode [-1,1]

Figure 3 shows snapshots of iso-surfaces of a vorticity quantity taken at several stages through the dissipation process. Here, the vorticity quantity is defined as:

$$\omega = \frac{\omega_z}{|\omega_z|} \times \left[\sum_{i=1}^{N} \omega_x + \sum_{i=1}^{N} \omega_y + \sum_{i=1}^{N} \omega_z \right] \tag{8}$$

Here, ω_z is the vorticity component in the axial direction, ω_x is the vorticity component in the direction parrallel to an imaginary line connecting the two vorticies, and ω_y is the vorticity component in the direction perpendicular to an imaginary line connecting the two vorticies; N is the number of planes in the axial direction (64 in the current investigation). Therefore, each summation term in equation 8 provides the mean value for each vorticity component in the axial direction ($\overline{\omega_x}$, $\overline{\omega_y}$ and $\overline{\omega_z}$ respectively). Note that the sign of ω_z is retained to identify which of the two primary vorticies that a vortex filament eminates from.

Figure 3A shows the flow field at the end of the linear growth period ($t^* = 16.65$). A low amplitude, sinuous oscillation is observed to act on each vortex. The lower vorticity iso-surfaces ($|\omega| = 0.5$) has an oscillation which is out of phase with the higher vorticity iso-surfaces ($|\omega| = 3.0$), this phenomena has been described in detail previously by [10], and is typical of a mode [-1,1] instability. Beyond this time, the perturbation continuous to grow, however higher order terms affect the flow and the growth is non-linear.

Figure 3B shows the flow field at $t^* = 20.25$. Here the growth is non-linear and has significantly altered the initial flow field. The higher vorticity iso-surfaces ($|\omega| = 3.0$) show large amplitude sinuous oscillations. At this stage, no vortex filaments, described by [10] as secondary vortices are evident for the iso-surface contours shown. However, the sinuous oscillations of the lower vorticity isosurfaces are in a direction parallel with an imaginary line connecting the two vortices.

Figure 3C shows the flow field at $t^* = 22.05$. The secondary vortices are apparent as vortex filaments emanating from one vortex core and wrapping around the opposing vortex core. These vortex filaments act to promote cross-vortex mixing and dissipate the vortex pair.

Figure 3D shows the flow field at $t^* = 23.4$. This is the time where the perturbation vorticity, defined as:

$$\eta = \sqrt{\sum (\omega - (\overline{\omega_x} + \overline{\omega_y} + \overline{\omega_z}))^2}, \tag{9}$$

is at its peak. The secondary vortices now dominate the flow field inducing significant mixing between the two vortex cores. Beyond this time η begins to reduce as the secondary vortices act to reduce the coherence of the two primary vortex cores.

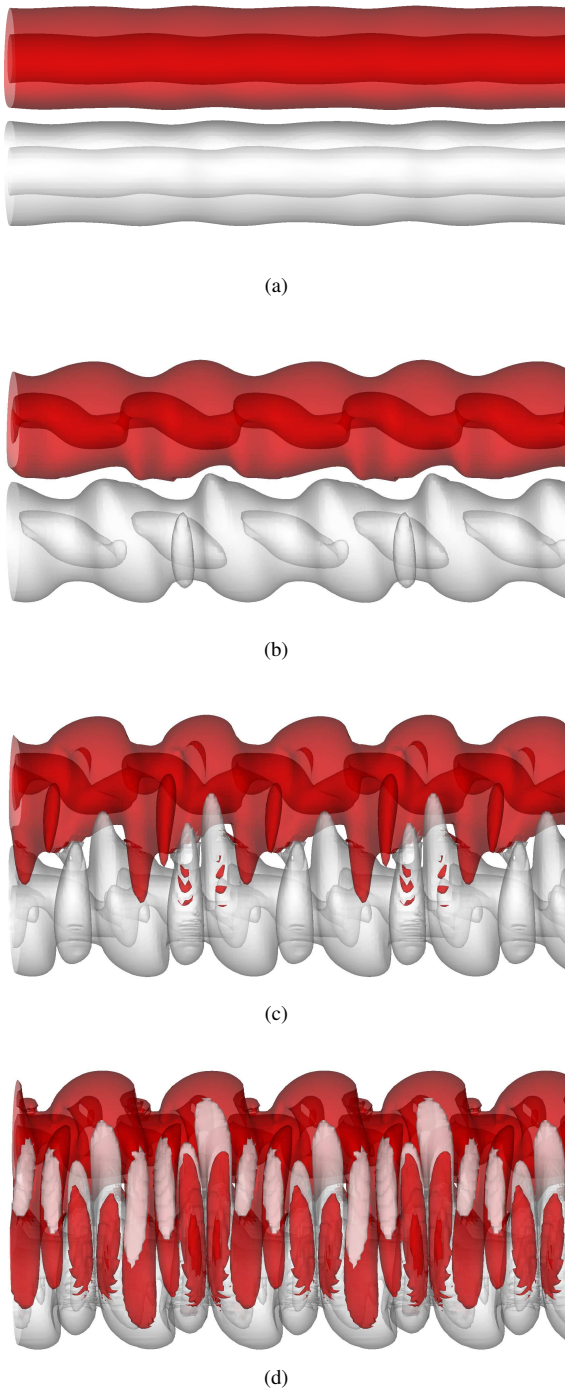

Figure 3: Snapshots showing isosurface contours of vorticity during the development of mode [-1,1]. The lower vorticity contours ($|\omega| = 0.5$) have been rendered semitransparent to reveal the upper vorticity contours ($|\omega| = 3.0$). Negative vorticity isosurfaces are shown in red, positive vorticity isosurfaces are shown in white. Snapshots correspond to: (a), $t^* = 16.65$; (b) $t^* = 20.25$; (c), $t^* = 22.05$; and (d), $t^* = 23.4$.

Figure 4 shows the growth in amplitude of the perturbation field, η, as a function of normalized time, t^*. The growth rate during the linear phase was found to be $\sigma^* \simeq 0.54$ which agrees well with the findings of [10, 5]. Differences in the growth rate between the studies may be attributed to the growth in the vortex radii as described by equation 4. This variation in growth rate, due to the variation in radii at early stages of the linear growth, has been discussed by [10, 6]. From $t^* \simeq 18$ the growth rate deviates from the linear growth rate as higher-order perturbation terms begin to affect the flow. The gradual reduction in the growth rate indicates that the mode is supercritical and is therefore not hysteretic as a function of Reynolds number. This is in agreement with prior theoretical studies of Kelvin mode development (for example see [10, 7]).

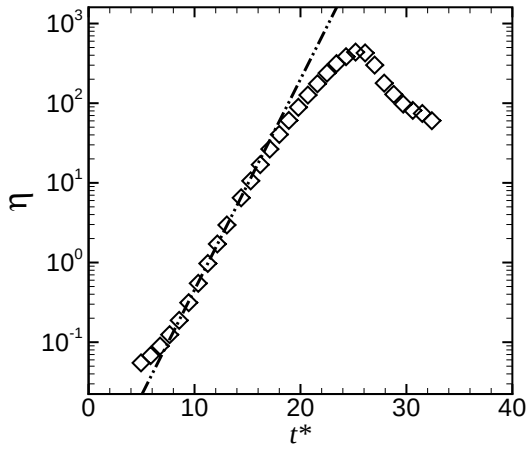

Figure 4: L_2 norm of the perturbation field for mode [-1,1] as a function of normalized time, t^* based on the perturbation vorticity. The dash-dot line represents the calculated linear growth rate.

Mode [-2,0]

The growth of mode [-2,0] was considered by setting $W_0 = 0.5$. This axial velocity coefficient has been shown previously (see [6] for details) to promote the highest growth rate for mode [-2,0].

Figure 5 shows snapshots of iso-surfaces of the vorticity taken at several stages through the dissipation process. Here, isosurfaces of $|\omega| = 2.5$ and $|\omega| = 0.5$ are considered. An instability is observed in both vortices, whose spatial structure differs significantly when compared to mode [-1,1]. This mode is a Kelvin mode of type [-2,0]. As with mode [-1,1], it is a coupling of two linear instability modes which are neutrally stable for an isolated vortex, but grow due to the influence of the second vortex. In this mode coupling the Kelvin mode 0 refers to a swelling and subsidence of the vortex core as a function of axis position. The Kelvin mode -2 refers to the braiding of positive and negative perturbation vorticity components within each vortex core. Thus, mode [-2,0] shows both these features.

Figure 5A shows the flow field at the end of the linear growth period ($t^* = 20.25$). Very little perturbation of the vortex pair is observed for the iso-surface levels considered. Here, the magnitude of the perturbation vorticity is significantly less than the base flow field. A minor oscillation is observed for $|\omega| = 2.5$ which is of the form of a swelling and subsidence of vorticity as a function of axis position consistent with a Kelvin mode 0.

Figure 5B shows the flow field at $t^* = 31.5$. Here, higher order perturbation components are growing in addition to the linear term and the perturbation growth rate is non-linear. The higher

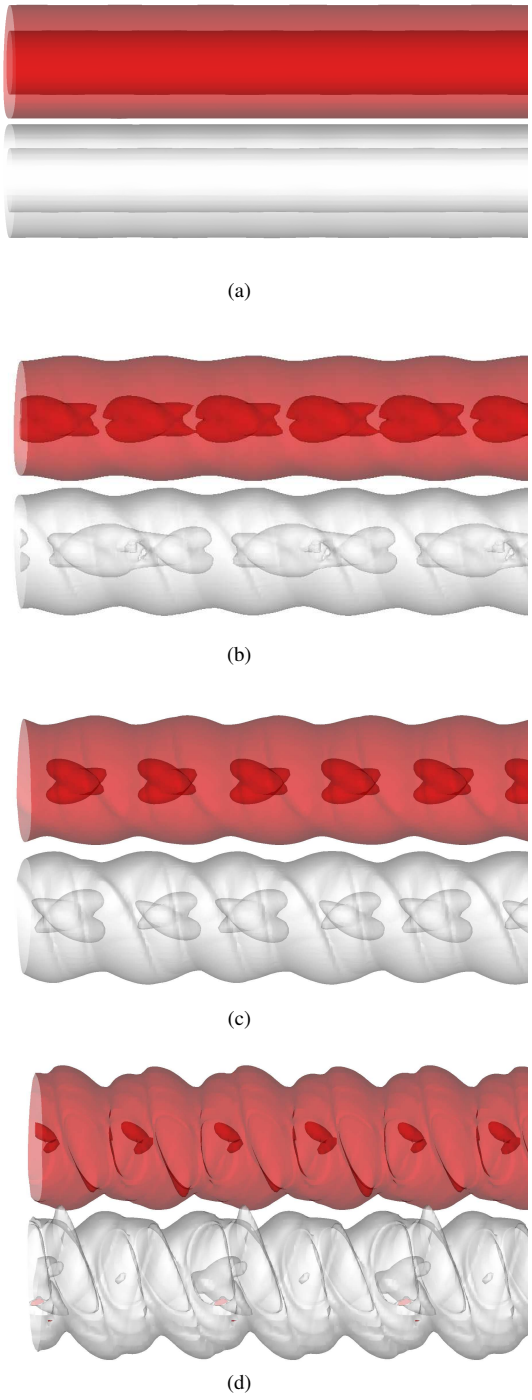

Figure 5: Snapshots showing isosurface contours of vorticity during the development of mode [-2,0]. The lower vorticity contours ($|\omega| = 0.5$) have been rendered semitransparent to reveal the upper vorticity contours ($|\omega| = 2.5$). Negative vorticity isosurfaces are shown in red, positive vorticity isosurfaces are shown in white. Snapshots correspond to: (a), $t^* = 20.25$; (b) $t^* = 31.5$; (c), $t^* = 33.75$; and (d), $t^* = 40.5$.

isosurface levels show the presence of both mode 0 and mode -2 in both vortex cores. Indeed, the higher vortex isosurface contours show that the vortices form a regular pattern of concentrated vorticity regions along the axis of the vortex. The strength of these vorticity regions dissipates over time (figures 5C and 5D).

Of interest, across the entire time series shown, no secondary vortices are observed to form between the two vortex cores. The vortices shown in figure 5D corresponding to $t^* = 40.5$ (the final time-step computed in the current set of computations), while significantly dissipated, remain highly coherent.

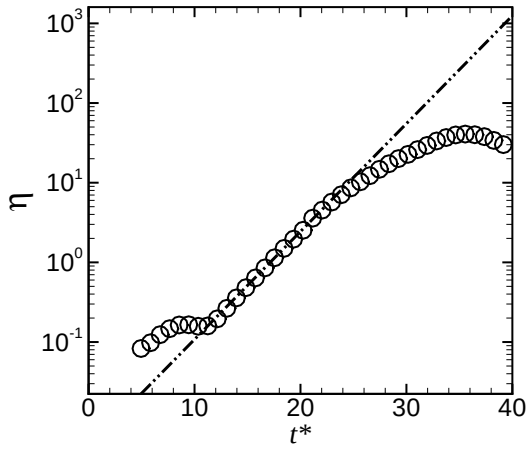

Figure 6: L_2 norm of the perturbation field for mode [-2,0] as a function of normalized time, t^* based on the perturbation vorticity. The dash-dot line represents the calculated linear growth rate.

Figure 6 shows the growth in amplitude of the perturbation field, η, as a function of normalized time, t^* for mode [-2,0]. The growth rate during the linear phase, $\sigma^* \simeq 0.33$ is significantly less than that for mode [-1,1], and approximately 0.3 times that which was predicted by [6]. However, the Reynolds numbers considered by [6] were significantly higher than that considered here which may explain the discrepency. From $t^* \simeq 24$ the growth rate deviates from the linear growth rate as higher-order perturbation terms begin to affect the flow. As with mode [-1,1] the gradual reduction in the growth rate indicates that the mode is supercritical and is therefore not hysteretic as a function of Reynolds number.

A Comparison of the Two Modes

In order to analyze the dissipation of the vortex pair under the influence of each instability mode we consider the variation in the mean circulation as a function of time for both instability modes (figure 7). Here, the vorticity is averaged in the axial direction across all 64 planes, and then integrated over an area surrounding the positive (right hand side) vortex to provide the circulation of that vortex. A significant difference is noted when comparing the two vortices, mode [-1,1] shows a significant decrease in mean circulation early in the non-linear growth period. Later in the non-linear growth region, the rate of change of mean circulation increases once more to the level noted in the linear growth region. The vortices subject to mode [-2,0] do not experience this dramatic reduction in mean circulation as the system moves from linear to non-linear growth.

It is postulated that the reduction in the circulation is due to the secondary vortices observed for the vortex pair subject to mode [-1,1]. Considering figure 7, the adjacent positive and negative vortex 'fingers' stretching between the vortex pair would act to significantly reduce the mean vorticity in the region where they

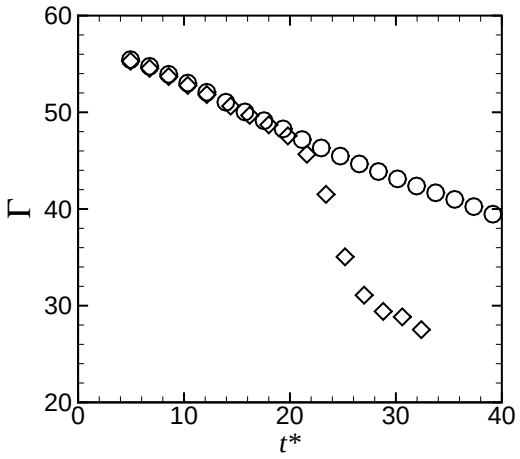

Figure 7: Mean value of circulation calculated in the region of the positive vortex per unit length as a function of normalized time. Diamonds represent measurements taken during the development of mode [-1,1]; circles represent measurements taken during the development of mode [-2,0].

occur.

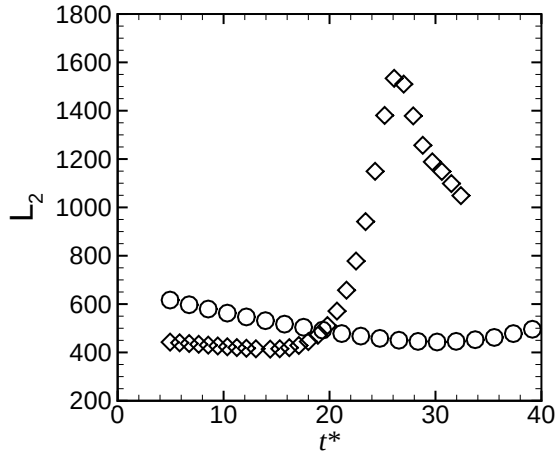

Figure 8: L_2 norm of circulation calculated in the region of the positive vortex per unit length as a function of normalized time. Diamonds represent measurements taken during the development of mode [-1,1]; circles represent measurements taken during the development of mode [-2,0].

In order to check this theory, the L_2 norm of the vorticity is determined (figure 8). Here the L_2 norm is defined as:

$$L_2 = \sqrt{\sum_{xz}\left[\sum_{i=1}^{N}\omega_x{}^2 + \sum_{i=1}^{N}\omega_y{}^2 + \sum_{i=1}^{N}\omega_z{}^2\right]} \qquad (10)$$

Where the term $\sum_{xz}$ indicates that the vorticity terms are summed in the $x\,y$ plane, to provide a single number representative of the vorticity norm. The summation is not taken across the entire domain. Instead we only consider the region around the positive vortex. As the L_2 norm considers the absolute value of the vorticity components, the secondary vortex structures will be summative and act to increase the L_2 norm. Figure 8 shows that this is indeed the case; as the growth rate moves from the linear to the non-linear phase, the L_2 norm increases substantially for the vortices subject to mode [-1,1].

The peak value of the L_2 norm occurs at $t^* \simeq 26$. The flow field corresponding to this is is shown in figure 9A. Of interest, the L_2 norm decreases at the same time as the rate of change of the mean circulation increases. Figure 9B shows a snapshot of isocontours of vorticity for $t^* = 32.85$. This corresponds to the final simulation computed for this mode in this study. Comparing figure 9A with figure 9B, we note that the strength of the secondary vortices decreases between these two images. Smaller scale structures begin to form between the secondary vortices.

By contrast, mode [-2,0] shows a gradual reduction in the L_2 norm; as the mode moves from a linear to a non-linear growth rate.

Implications of the Current Findings

Several interesting points are noted with respect to the ability of both mode [-1,1] and mode [-2,0] to enhance the reduction of the coherent circulation of the vortex pair. The first is that mode [-1,1] clearly enhances vortex dissipation with much greater effect than mode [-2,0]. This is despite both modes having comparable growth rates in the linear regime. The reason for this significant difference in growth rate is due to the lack of secondary vortices noted for mode [-2,0]. These secondary vortices act to provide mixing within each vortex reducing the coherence of the vortical structures. The secondary vortices grow as a result of the sinusoidal nature developed during the linear growth period of mode [-1,1]. By contrast, mode [-2,0] does not exhibit a sinuous growth resulting in no non-linear 'communication' between the principal vortices. As a result, no inter-vortical mixing is noted. Mode [-2,0] appears to reach a stable state with successive vortical nodes along the axis of each vortex core. These nodes do not appear to exhibit further instabilities at these low Reynolds numbers, and the coherent nature of the vortices is preserved.

It is also intersting to note that the prediction of a large growth rate during the linear phase of development is not sufficient to ensure the success of a Kelvin type mode to enhance vortex dissipation. A secondary requirement is that of inter-vortical mixing. This has implications for the selection of linear modes for enhanced vortical dissipation

Conclusions

The growth of instabilities leading to the dispersion of a Batchelor vortex pair has been considered. In particular, the linear and non-linear growth of two Kelvin modes were considered. It was noted that while the instability modes had comparable linear growth rates, the dissipation of the vortex cores varied significantly. Simulations of mode [-1,1] had secondary vortices (vortex filaments stretching between the vortices constituting the vortex pair) which significantly enhanced dissipation. mode [-2,0] did not have secondary vortices, and the vortices maintained a coherent structure well after the linear growth period was complete. A large growth rate during the linear phase of development is not sufficient to ensure the success of a Kelvin type mode to enhance dissipation of a vortex pair.

Acknowledgements

The authors would like to acknowledge Mark Thompson for providing the numerical code used and the strong support from the Australian Partnership for Advanced Computing (APAC)

which enabled this research to take place.

(a)

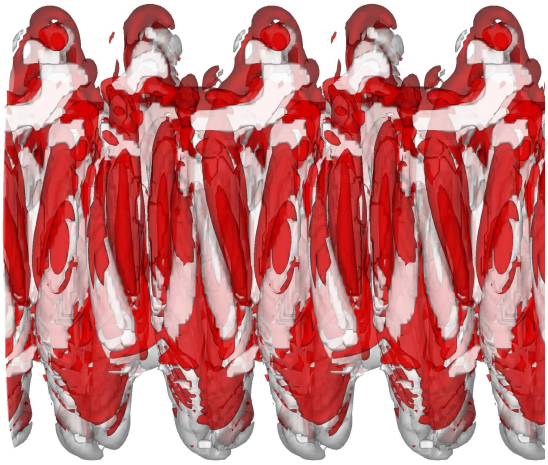

(b)

Figure 9: Snapshots showing the final isosurface contours of vorticity computed for mode [-1,1] during the final stages of vortex interaction computed in this study. Snapshots correspond to: (a), $t^* = 26.1$; and (b), $t^* = 32.85$. The lower vorticity contours ($|\omega| = 0.5$) have been rendered semitransparent such that upper vorticity contours ($|\omega| = 3.0$) are visible. Negative vorticity isosurfaces are shown in red, positive vorticity isosurfaces are shown in white.

References

[1] Batchelor, G. K., Axial flow in trailing line vortices *J. Fluid Mech.*, **20**, 1964, 645-658.

[2] Crow, S. C., Stability theory for a pair of trailing vortices. *AIAAJ.*, **8**, 1970, 2172-2179.

[3] Fabre, D., Sipp, D. and Jacquin, L., Kelvin waves and the singular modes of the Lamb-Oseen vortex *J. Fluid Mech.*, **551**, 2006, 235–274.

[4] Karniadakis, G. E., Israeli, M., and Orszag, S. A., High-order splitting methods for the incompressible Navier-Stokes equations*J. Comp. Phys.*, **97**, 1991, 414–443.

[5] Laporte, F., Elliptic instability of counter-rotating vortices: Experiment and direct numerical simulation *AIAA J*, **40**, 2002, 2483–2494.

[6] Lacaze, L., Ryan, K. and Le Dizès, S., Elliptic instability in a strained Batchelor vortex *J. Fluid Mech.*, **577**, 2007, 341–361.

[7] Le Dizès, S. and Laporte, F., Theoretical predictions for the elliptical instability in a two-vortex flow *J. Fluid Mech.*, **471**, 2002, 169–201.

[8] Le Dizès, S. and Lacaze, L., An asymptotic description of vortex Kelvin modes *J. Fluid Mech.*, **542**, 2005, 69–96.

[9] Le Dizès, S. and Verga A., Viscous interactions of two co-rotating vortices before merging *J. Fluid Mech.*, **467**, 2002, 389–410.

[10] Leweke, T. and Williamson, C. H. K., Cooperative elliptic instability of a vortex pair *J. Fluid Mech.*, **360**, 1998, 85–119.

[11] Meunier, P. and Leweke, T., Elliptic instability of a co-rotating vortex pair *J. Fluid Mech.*, **533**, 2005, 125–159.

[12] Olwi, I. and Ghazi, M., Effect of wing tip vortices on a trailing aircraft *AIAA J*, **30**, 1992, 2186–2187.

[13] Ryan, K., Sheard, G.J. and Thompson, M.C., Short wave instabilities of counter-rotating Batchelor vortex pairs, in *Proceedings of the Fifth International Conference on CFD in the Process Industries, CSIRO Australia*, editors P.J. Witt and P. Schwarz, Hilton on the Park, Melbourne, Australia, 2006, 170Rya.

[14] Sipp, D., Jacquin, L. and Cosssu, C., Self-adaptation and viscous selection in concentrated two-dimensional dipoles, *Phys. Fluids*, **12**, 2000, 245–248.

[15] Spalart, P., Airplane trailing vortices. *Annu. Rev. Fluid Mech.*, **30**, 1998, 107–138.

[16] Thompson, M.C., Hourigan, K. and Sheridan, J., Three-dimensional instabilities in the wake of a circular cylinder, *Exp. Therm. and Fluid Sci.*, **12**, 1996, 190–196.